
Interaction of Jets with Galactic Winds

Martin Krause and Max Camenzind

Landessternwarte Königstuhl 69117 Heidelberg, Germany
M.Krause@lsw.uni-heidelberg.de

We have used the vectorised and parallelised magnetohydrodynamics code NIRVANA on the NEC SX-5 and the new SX-6 installation in parallel mode to simulate the interaction of jets with a galactic wind that might be typical for the star-bursting radio-galaxies of the early universe.

The two simulations, one axisymmetric and one in 3D show that the jet pierces and destroys a thin and dense shell produced by the pre-installed superwind.

We suggest that small radio galaxies at high redshift might be absorbed on the blue wing due to the galactic wind shell, and possibly on the red wing due to a cooling flow. In larger sources the jet cocoon will fill the wind cavity and accelerate the shell. The Rayleigh-Taylor instability will then disrupt the shell and disperse dense, possibly star-forming fragments throughout the region.

1 Introduction

Radio galaxies are associated with an enormous release of energy, exceeding 10^{40} Watts (Ghisellini 2003; Krause & Camenzind 2003). From the power house in the center of certain galaxies, where supermassive black holes of billions of solar masses are believed to reside, the power is channeled through narrow jets out to distances of several million light years, far outside of the host galaxy. They stimulate emission throughout the electromagnetic spectrum that can be observed up to the largest distances of the visible universe. Being the likely progenitors of today's brightest cluster galaxies (Carilli et al. 2001), radio galaxies at high redshift mark the peaks of highest density in the early universe, and highlight the formation of galaxy clusters.

At redshifts of $z > 0.6$ extended optical continuum and emission line regions, aligned with the radio structures, become prominent companions (McCarthy 1993). Beyond a redshift of $z \approx 2$, most of the optical emission originates from the Lyman α transition of hydrogen. Huge Ly α halos have been observed in the young universe (e.g. Reuland et al. 2003). Their size often

exceeds the radio size. Only for radio extents smaller than 50 kpc^1 , the Ly α emission, that has turbulent velocities of typically 1000 km/s , is totally absorbed with a velocity width of several 10 km/s (van Ojik et al. 1997). The absorbers are typically blue-shifted (van Ojik et al. 1997; De Breuck et al. 2000).

Optical emission lines are produced by clouds at temperatures of 10^4 to 10^5 K . These are thought to be embedded in thin and hot plasma in pressure equilibrium. The emitting gas is either ionised by ultraviolet radiation, e.g. from hot stars or the central quasar, or collisionally excited due to shocks associated with the jet expansion. The location of the absorbing screen is still a matter of debate. Based on the determination of differing metallicities in the emitting and absorbing gas components, some authors have suggested an extended low density shell around these systems (Binette et al. 2000; Jarvis et al. 2003; Wilman et al. 2003). This has the disadvantage that the low velocity width of the absorbers seems to be hard to explain. Based on hydrodynamic simulation, one of the authors has suggested a different model (Krause 2002). According to that, the emission line region is surrounded by a high density shell. This shell is formed when the gas behind the leading bow shock is dense enough to cool on the propagation time-scale. This part of the gas loses pressure support and is compressed in a thin and dense shell that would produce the observed absorption. The latter model may produce too much luminosity in the Ly α and X-ray channel. The combination of a jet with a galactic wind is similar to the that model with the exception that lower luminosities of the absorbing shells are involved.

The jet–galactic wind interaction scenario is detailed in sect. 2, followed by a discussion of the computational aspects in sect. 3. We present the results of the simulations in sect. 4. They are discussed in sect. 5.

2 Details of the interaction of an extragalactic jet with a galactic wind.

This model (compare Fig. 1) starts with a starburst. This means that the stellar winds and supernovae inject gas and energy into the interstellar medium, which leads to an outflow of gas. The outflow is headed by a bow shock (Fig. 1a). After the cooling time, the material behind this shock will cool and form a dense shell (Fig. 1b), which may absorb emission from gas inside of the shell. The shell may be Rayleigh-Taylor unstable and some gas may fall back. Additionally, ejecta from the stars of the galaxy fill the cavity. When the jet starts (Fig. 1c), the gas inside of the cavity may be excited to emit strong Ly α due to photoionisation by the central quasar, which has to be assumed to be active when it ejects jets, or by shocks associated with the jet expansion. This emission will be absorbed on the blue wing due to the expanding shell,

¹ $\text{kpc} = 3260 \text{ light years} = 3 \times 10^{19} \text{ m}$

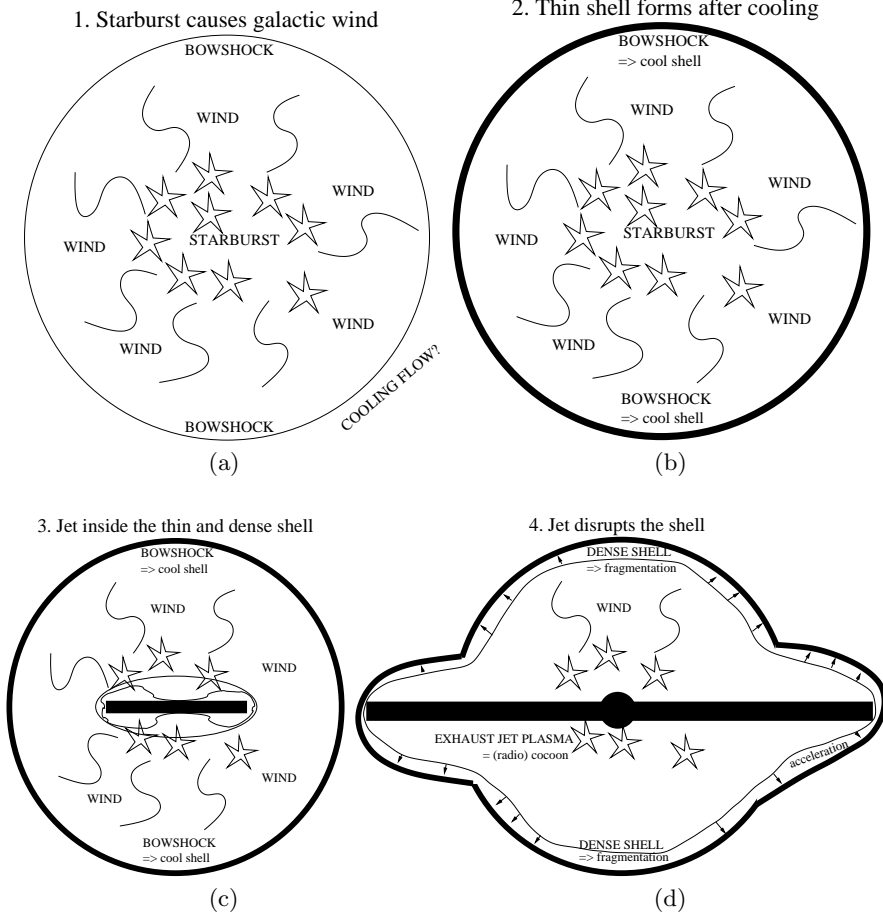


Fig. 1. Sketch of the interaction of a jet with a galactic wind adopted here. First, the supernovae associated with a starburst produce a galactic wind (a). After the cooling time, the gas inside of the bow shock cools and forms a dense shell (b). The shell may become Rayleigh-Taylor unstable and loose some material to the inside. Then, the jet starts (c). The stars still eject gas which forms an emission line region by photoionisation or jet induced shocks. The thin and dense shell absorbs at a narrow velocity range. We suggest the small radio galaxies to be in this phase. When the jet pierces the shell and the exhaust jet plasma fills the cavity, the shell is accelerated because of the high pressure in the interior (d). The shell is then disrupted because of the greatly enhanced Rayleigh-Taylor instability. The fragments are likely to form stars. Radio galaxies bigger than 50 kpc are suggested to be in that phase. In every phase, a cooling flow may exist that may form an infalling dense shell immediately outside of the wind’s bow shock.

and also possibly on the red wing due to an infalling cooling flow. Eventually, the jet plasma will fill all of the cavity (Fig. 1d). The enhanced pressure will accelerate the bow shock of the wind, which merges with the jet’s bow shock at that time. This causes the shell to be highly Rayleigh-Taylor unstable, and the shell will be disrupted quickly. Additionally, the beams pierce it. The shell fragments will fly around in a turbulent way and are likely to form stars.

This scenario was examined by hydrodynamic simulations, which is reported on in the following.

3 Computational aspects

3.1 Numerics

For the computations in this contribution, the magneto-hydrodynamic (MHD) code *Nirvana* was employed (Ziegler & Yorke 1997). In that version, it solves the MHD equations in three dimensions (3D) for density ρ , velocity \mathbf{v} , internal energy e , and magnetic field \mathbf{B} :

$$\frac{\partial \rho}{\partial t} + \nabla \cdot (\rho \mathbf{v}) = 0 \quad (1)$$

$$\frac{\partial \rho \mathbf{v}}{\partial t} + \nabla \cdot (\rho \mathbf{v} \mathbf{v}) = -\nabla p - \rho \nabla \Phi + \frac{1}{4\pi} (\mathbf{B} \cdot \nabla) \mathbf{B} - \frac{1}{8\pi} \nabla \mathbf{B}^2 \quad (2)$$

$$\frac{\partial e}{\partial t} + \nabla \cdot (e \mathbf{v}) = -p \nabla \cdot \mathbf{v} - \rho^2 \Lambda \quad (3)$$

$$\frac{\partial \mathbf{B}}{\partial t} = \nabla \times (\mathbf{v} \times \mathbf{B}) \quad , \quad (4)$$

where Φ denotes an external gravitational potential and Λ is a temperature dependent cooling function (zero metals, zero photoionising field) according to Sutherland & Dopita (1993). NIRVANA can be characterised by the following properties:

1. explicit Eulerian time-stepping,
2. operator-splitting formalism for the advection part of the solver,
3. method of characteristics-constraint-transport algorithm to solve the induction equation and to compute the Lorentz forces;
4. artificial viscosity has been included to dissipate high-frequency noise and to allow for shock smearing in case the flow becomes supersonic.

The code was vectorised and parallelised by OpenMP like methods, and successfully run on the SX-5 (Krause & Camenzind 2002). All the significant loops could be vectorised. The number crunching part scales without significant performance loss. This is also true for the MHD part of the solver. The code was now modified slightly in order to run on the new NEC SX-6 installation of the HLRS. A profile output for a test run is shown in table 1. The test run evolved a hydrodynamic problem on a 4096×4000 grid for 100 timesteps.

Table 1. Profile output: SX-6 test run

Real Time (sec)	: 192.397907	User Time (sec)	: 771.848942
Sys Time (sec)	: 2.102633	Vector Time (sec)	: 672.636268
Inst. Count	: 58955512397	V. Inst. Count	: 23660611300
V. Element Count	:6053551438274	FLOP Count	:2494019257489
MOPS	: 7888.650237	MFLOPS	: 3231.227151
MOPS (concurrent)	: 57155.158190	MFLOPS (concurrent)	: 23411.013720
A.V. Length	: 255.849325	V. Op. Ratio (%)	: 99.420335
Memory Size (MB)	: 2320.000000	Max Concurrent Proc.	: 8
Conc. Time(>= 1) (sec):	106.531878	Conc. Time(>= 2) (sec):	95.892731
Conc. Time(>= 3) (sec):	95.830364	Conc. Time(>= 4) (sec):	95.813671
Conc. Time(>= 5) (sec):	95.798599	Conc. Time(>= 6) (sec):	95.782837
Conc. Time(>= 7) (sec):	95.603244	Conc. Time(>= 8) (sec):	90.646246
Event Busy Count	: 0	Event Wait (sec)	: 0.000000
Lock Busy Count	: 17078	Lock Wait (sec)	: 5.299937
Barrier Busy Count	: 0	Barrier Wait (sec)	: 0.000000
MIPS	: 76.382190	MIPS (concurrent)	: 553.407238
I-Cache (sec)	: 0.408468	O-Cache (sec)	: 6.734071
Bank (sec)	: 21.394816		

This output indicates a performance of roughly 23 GFlop for a run with 8 processors and an acceptable load ballancing. A single processor run yielded 3.5 GFlops. This is 38% of the peak performance of 9.2 GFlops. A critical point in achieving this quite good performance was a change in the upwind part of the advection solver. Now, both directions are computed, and the one needed is selected afterwards. This saves an if-clause in the vectorised loops. Although, more floating point operations are performed, the speed increase is sufficiently high. The code scales well with the number of processors within one node (Fig. 2).

We report to computations. An axisymmetric simulation has been performed on one processor of the SX-5, involving about 200 CPU hours and 200 MB of memory. Also, a fully 3D computation has been carried out on two processors of the SX-6, involving 100 CPU hours and 2 GB of memory. The main reason for the short computation time is the limit of 100 CPU hours for the batch queue on the SX-6 and the fact that the machine was installed only two weeks ago at the time of writing. We typically need some 1000 CPU hours for a full run. Also this run is currently repeated on the SX-5 and evolved for a longer time.

3.2 Setup

We start the computations with an isothermal (10^6 K) King profile for the initial density ρ_e :

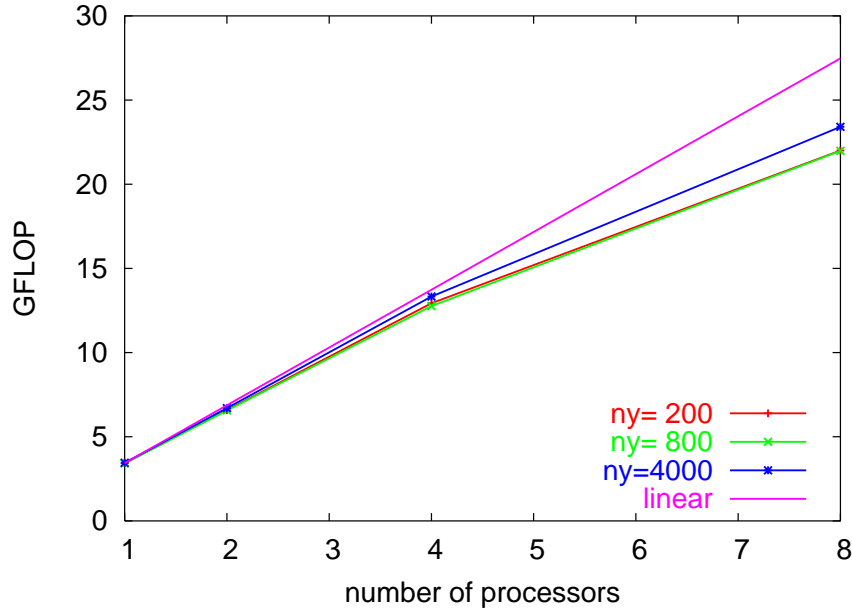


Fig. 2. Scaling of the NIRVANA code on the new SX-6 installation at HLRS

$$\rho_e = 0.3m_p \left[1 + \left(\frac{r}{10 \text{ kpc}} \right)^2 \right]^{-1}, \quad (5)$$

where r is the spherical radius. The atmosphere is stabilised by the background gravity of the dark matter halo in hydrostatic equilibrium. We start the galactic wind by injecting mass at a rate $\dot{M} = 10M_\odot/\text{yr}$ and thermal energy at a rate $L_g = 10^{51}$ erg/yr, which corresponds to one supernova per year, inside a region of 3 kpc, with an exponential decay. For the 2.5D run (axisymmetry), the grid has 2047×1023 points that correspond to 200×100 kpc. In the 3D case, the grid has $511 \times 201 \times 201$ points, corresponding to $200 \times 80 \times 80$ kpc. With a jet radius of one (two) kpc the resolution corresponds to 10 (5) points per beam radius for the 2.5D (3D) case. In both cases, the resolution is enough to resolve the radiative bow shock.

After 80 Myrs, when the dense shell has formed, bipolar jets are injected in the center of the galaxy which also corresponds to the center of the grid. The jet density is $10^{-5}m_p \text{ cm}^{-3}$. This is roughly a hundred times less than the gas inside of the wind bubble at the time of the jet start. The jets are then evolved for 18 (2) Myrs.

4 Simulation results

4.1 Axisymmetric simulation

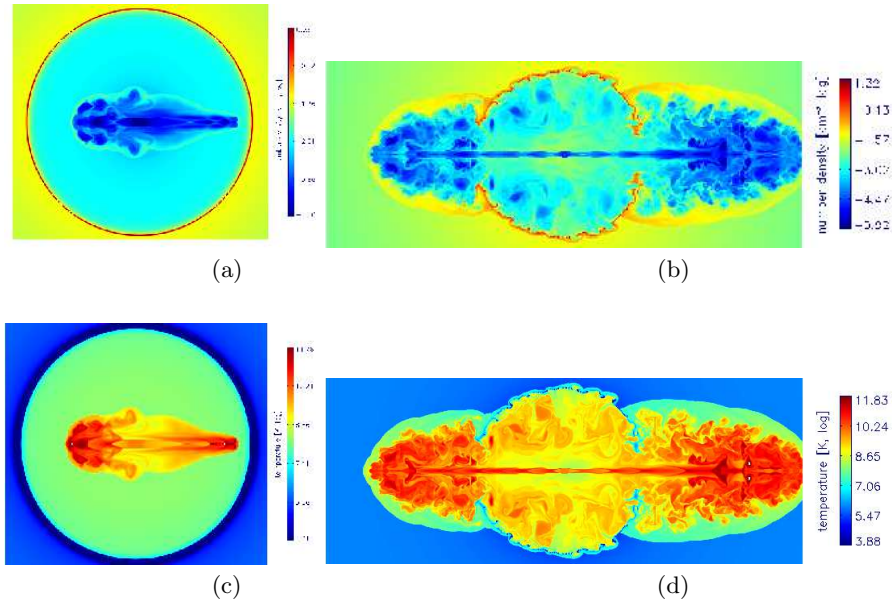


Fig. 3. Representation of number density (top) and temperature (bottom) distribution for the 2.5D run, at 80.5 (left) and 95 Myr (right).

Density and temperature maps of the 2.5D simulation are shown at two different times in Fig 3. In the earlier plots, the jet is well inside the spherically symmetric galactic wind. This wind has already formed a dense shell before the start of the jet. Careful inspection of Fig 3c reveals the shell to have a temperature of 10^4 K, with a thin enhancement to $\approx 10^5$ K in the middle. This is the position of the bow shock. The structure can be seen in more detail in Fig 4. The bow shock of the galactic wind expands into a cooling flow. The shock, at 400 km/s, heats the gas to $> 10^5$ K. Inside of the shock, the gas cools quickly down to 10^4 K, the lower end of the cooling function. Outside of the shock, the cooling flow has also produced a cool and dense shell, inflowing at ≈ 100 km/s. The two jets pierce a considerable hole into these shells. When the jet's bow shock hits the one of the wind, the shell gets accelerated. This shell can only remain stable as long as its deceleration exceeds the local gravity. An acceleration greatly enhances the Rayleigh-Taylor instability. Hence, a considerable amount of gas is entrained. Fig. 3b shows this entrained gas in yellow-green colors, extending in fingers from the shell down to the jet beam, where it assembles due to gravity. The shell is transformed into clumps that

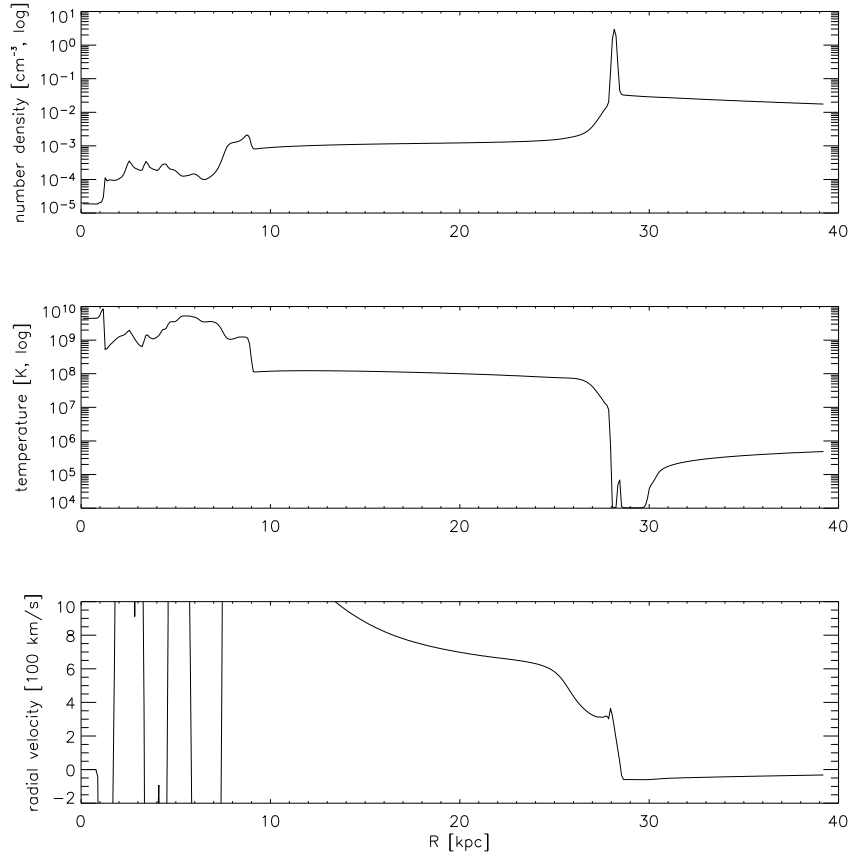


Fig. 4. Slice of density, temperature and sideways velocity for the 2.5D run at 80.5 Myr. The slice is located vertical to the jet in the center. The bow shock is located at $R = 29$ kpc. Inside of it the collapsed shell flows outward at ≈ 400 km/s, outside of it cool gas flows in at ≈ 100 km/s.

still get denser at the end of the simulation. A magnification of the bow shock region in Fig. 3d is shown in Fig. 5. The fragments of the shell can be seen in blue. Between the fragments, the very hot (red) jet plasma, that was injected through the beams and distributed in the wind cavity, flows past and compresses the ambient gas, which drives a faster, non-radiative bow shock.

The dissolution of the shell can also be seen from the number density versus sideways velocity histograms (Fig 6). At 80.5 Myr, the motion of the dense gas is well ordered, centered at 200 km/s. At 95 Myr, higher densities and higher velocities are present, but the distribution is much less uniform.

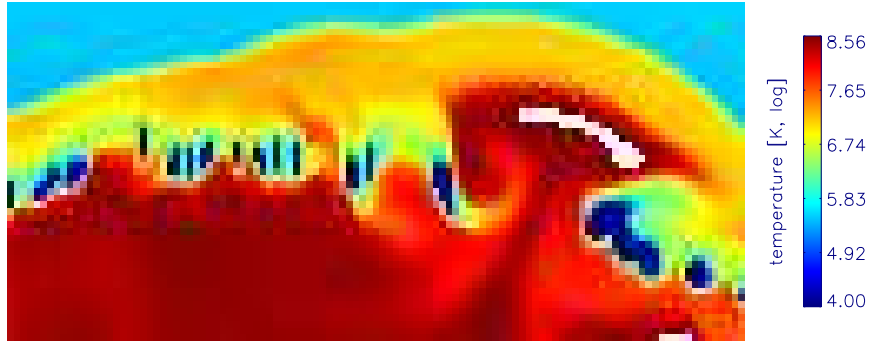


Fig. 5. Magnification of the bow shock region of Fig. 3d. The highest temperature has the exhaust plasma from the jet beam. This plasma (hot, red) flows through the holes between the fragments (cold, blue) of the shell and compresses the ambient gas thereby establishing a new, non-radiative bow shock. The highest temperature is shown in white.

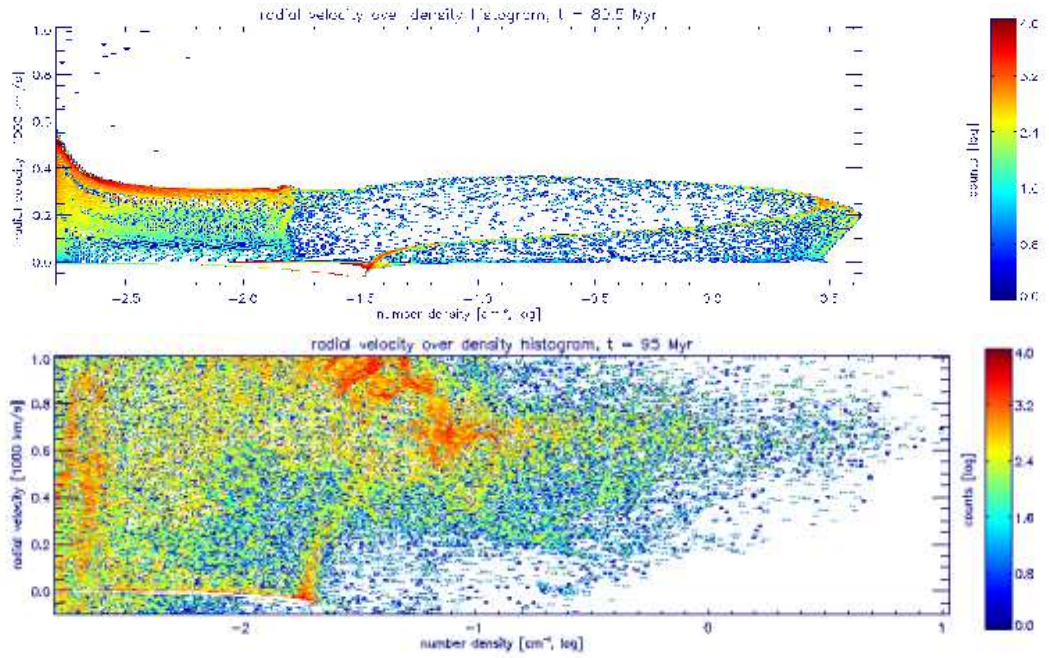


Fig. 6. Frequency of number densities and sideways (radial) velocities at 80.5 Myr and 95 Myr. The counts are cut at 10^4 .

4.2 Three-dimensional simulation

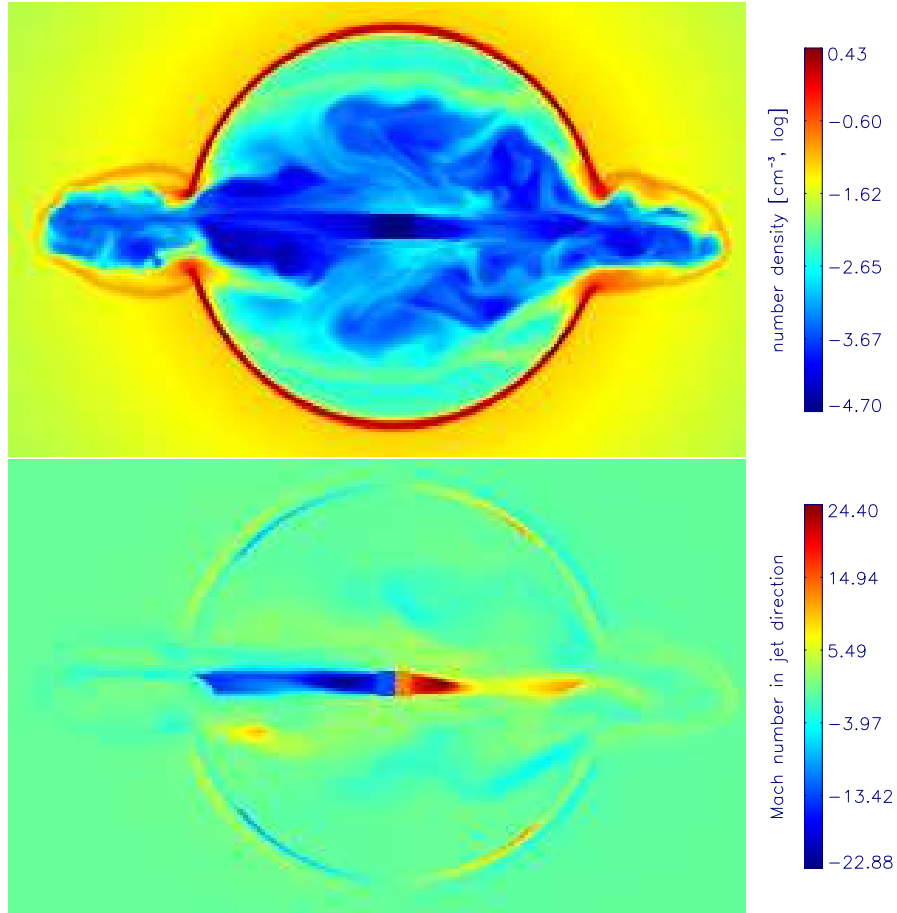


Fig. 7. Density (top) and Mach number in jet direction (bottom) for the 3D simulation at 82 Myr.

The jets in the 3D run stay quite symmetric. Only the cocoon shows some three-dimensional structure. The bow shock of the jet has unfortunately not yet reached the wind's bow shock, and the process of fragmentation can therefore not yet be compared to the 2.5D case. An interesting result is that the Mach number drops considerably at the location of the shell.

5 Discussion

The simulations show that a jet is able to disrupt a wind blown shell via the Rayleigh-Taylor instability during the simulation time. This was shown directly in density contour plots, as well as the histograms of velocity versus number density. The 3D computation has not yet been evolved for long enough in order to compare the fragmentation process. Another interesting feature to appear in 3D is jet bending. Slight changes of the jet direction might cause the beam to hit the shell on one side, which may deflect it. This effect is absent, the beams stay straight. An emission line region within such a bubble would first be absorbed on the blue wing, and if a cooling flow is present, possibly also on the red wing. Observed radio galaxies in the young universe are absorbed preferentially on the blue wing. This indicates that, if the suggested scenario is correct, the gas around most of these objects is either less dense or has a higher temperature, in order not to show a cooling flow. However, the properties of the environments of these objects seem to be quite uniform (van Ojik et al. 1997), because of the strict absence of absorbers for objects larger than 50 kpc, and the presence in nearly all of the objects smaller than that. It is therefore likely that they are located at the border line. An inflowing cool shell will be created when the cooling time for the ambient gas is shorter than the delay between starburst and jet start ($\approx 10^8$ years):

$$10^8 \text{ yr} = t_{\text{cool,ambient}} = 12 \text{ Myr} \sqrt{T/10^7 \text{ K}} / (n/\text{cm}^{-3}) \quad (6)$$

For the gas inside of the wind's bow shock to cool, the shock's Mach number should be close to unity. Since absorbers are typically blue-shifted by a few hundred km/s, it follows:

$$200 \text{ km/s} \approx c_{\text{sound,ambient}} = 400 \text{ km/s} \sqrt{T/10^7 \text{ K}} \quad (7)$$

These two requirements fit together, if the ambient densities are roughly 0.1 cm^{-3} , and the temperature is typically about 10^6 K , i.e. the galaxy clusters in the young universe would have had denser and colder gas than nearby ones.

This comparison, and the simulation results achieved on the NEC SX-5 and SX 6 supercomputers at the HLRS suggest that high redshift radio galaxies may indeed be associated with thin shells blown by a galactic wind.

Acknowledgments

This work was also supported by the Deutsche Forschungsgemeinschaft (Sonderforschungsbereich 439).

References

- Binette, L., Kurk, J. D., Villar-Martín, M., & Röttgering, H. J. A. 2000, *A&A*, 356, 23
- Carilli, C. L., Miley, G., Röttgering, H. J. A., Kurk, J., Pentericci, L., Harris, D. E., Bertoldi, F., Menten, K. M., & van Breugel, W. 2001, in *Gas and Galaxy Evolution*, ASP Conference Proceedings, Vol. 240. Edited by John E. Hibbard, Michael Rupen, and Jacqueline H. van Gorkom, San Francisco.
- De Breuck, C., Röttgering, H., Miley, G., van Breugel, W., & Best, P. 2000, *A&A*, 362, 519
- Ghisellini, G. 2003, *New Astronomy Review*, 47, 411
- Jarvis, M. J., Wilman, R. J., Röttgering, H. J. A., & Binette, L. 2003, *MNRAS*, 338, 263
- Krause, M. 2002, *A&A*, 386, L1
- Krause, M. & Camenzind, M. 2002, in *High Performance Computing in Science and Engineering '01*, eds.: Krause, E. and Jäger, W., Springer, 329+
- Krause, M. & Camenzind, M. 2003, *New Astronomy Review*, 47, 573
- McCarthy, P. J. 1993, *A&A Review*, 31, 639
- Reuland, M., van Breugel, W., Röttgering, H., de Vries, W., Stanford, S. A., Dey, A., Lacy, M., Bland-Hawthorn, J., Dopita, M., & Miley, G. 2003, *ApJ*, 592, 755
- Sutherland, R. S. & Dopita, M. A. 1993, *ApJ Supplement*, 88, 253
- van Ojik, R., Röttgering, H. J. A., Miley, G. K., & Hunstead, R. W. 1997, *A&A*, 317, 358
- Wilman, R. J., Jarvis, M. J., Röttgering, H. J. A., & Binette, L. 2003, *New Astronomy Review*, 47, 279
- Ziegler, U. & Yorke, H. W. 1997, *Computer Physics Communications*, 101, 54